

SCIENTIFIC REPORTS

OPEN

Link between concentrations of sediment flux and deep crustal processes beneath the European Alps

Philippos Garefalakis & Fritz Schlunegger

Received: 16 August 2017

Accepted: 20 November 2017

Published online: 09 January 2018

Large sediment fluxes from mountain belts have the potential to cause megafans to prograde into the neighbouring sedimentary basins. These mechanisms have been documented based from numerical modelling and stratigraphic records. However, little attention has been focused on inferring temporal changes in the concentrations of supplied sediment from coarse-grained deposits. Here, we extract changes of this variable in the field from a Late Oligocene, c. 4 km-thick suite of fluvial conglomerates situated in the North Alpine foreland basin, which evolved in response to the tectonic and erosional history of the Alps. We measure a decrease in channel depths from >2 m to <1 m and an increase in the largest grain sizes from <15 cm to >20 cm from the base to the top of the suite. These constraints are used to calculate an increase in fan surface slopes from $<0.3^\circ$ to $>1.0^\circ$ based on the Shields criteria for sediment entrainment. We combine slope and bulk grain size data with the Bagnold equation for sediment transport to infer higher concentrations of the supplied sediment. We use these shifts to propose a change towards faster erosion and a steeper landscape in the Alpine hinterland, driven by mantle-scale processes beneath the Alps.

Sediment flux has been considered as one of the major variables controlling the dispersion of sediment in sedimentary basins^{1–3} and has likewise assigned a primary role in regulating the fluvial style particularly in terrestrial environments⁴. In this context, it has been proposed that larger sediment fluxes tend rivers to adapt a braided pattern, while lower sediment discharge is commonly, but not always, associated with streams that are laterally confined by floodplains⁴. In the same sense, larger supply rates of sediment are capable of shifting sedimentary depocenters towards more distal sites, while reductions of sediment fluxes are commonly associated with a back-stepping of sedimentary environments towards their sedimentary sources^{1,5}. These mechanisms have been well documented from modern sedimentary systems and have particularly been inferred from stratigraphic records of coarse-grained clastic depocenters^{3,6}, and they are decently well understood based on conceptual work^{1,5}. However, sediment flux not only comprises a volumetric measure of the supplied grains, but it also includes the calibre and the concentration of this material⁴. While much attention has been paid on how shifts in grain size populations are recorded in sedimentary records, and on how these signals propagate through terrestrial environments^{7–14}, much less research has been directed towards inferring possible changes in the concentrations of supplied sediment from stratigraphic records. However, because higher sediment concentrations in streams are consequences of faster erosion in the source area, as modern examples have shown¹⁵, this variable contains valuable information about the erosional processes that are dominant in the specific high relief erosional zone. Here, we extract sedimentary information from coarse-grained fluvial conglomerates that we use as a basis to infer changes in the concentrations of the supplied sediment. We focus on a suite of Late Oligocene conglomerates situated in the North Alpine foreland basin, which evolved in response to the tectonic and erosional history of the Alps. We use these shifts to propose a transient surface response of the Alpine landscape to fast rock uplift, driven by mantle-scale processes situated in the deep Earth beneath the Central Alps of Switzerland.

The Swiss Alps (Fig. 1a) can be characterized as a doubly-vergent mountain belt with a crystalline core exposed in back of the orogen that is flanked by N- and S-vergent thick-skinned and thin-skinned thrusts¹⁶. The present-day litho-tectonic architecture of the Alps resulted from the subduction-collision history between

University of Bern, Institute of Geological Sciences, Baltzerstrasse 1+3, CH-3001, Bern, Switzerland. Correspondence and requests for materials should be addressed to P.G. (email: philippos.garefalakis@students.unibe.ch)

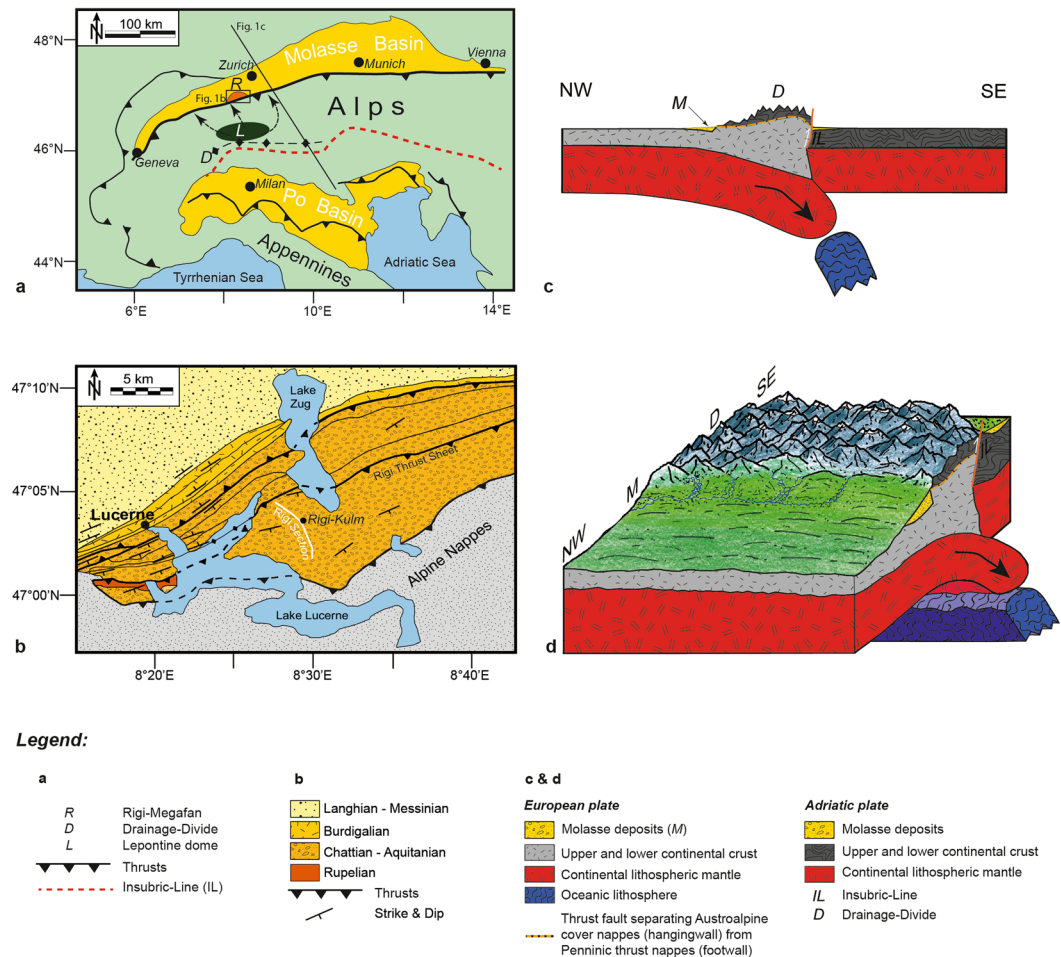


Figure 1. The Alps and their geodynamic state during the Late Oligocene. **(a)** Geologic map of the Alps and the neighbouring sedimentary basins²³. The map also shows the location of the Rigi megafan (denoted as R) that was sourced from the area surrounding the Lepontine area (denoted as L) in the Central Alps of Switzerland. D denotes the major Alpine drainage divide between c. 30–20 Ma. **(b)** Simplified geologic map of the Rigi area, situated on the northern side of the Alps²². Please see Fig. 1a for location of map. **(c)** Schematic section through the Alps²³ illustrating the geodynamic situation between c. 30–20 Ma. At that time, the Alps were made of the orogenic lid constituted by the Austroalpine nappes, and the crystalline core that assembled lithologies of the Penninic nappes. Slab breakoff beneath the rear of the Alps resulted in a period of fast rock uplift and in the formation of a highly elevated topography. Please see Fig. 1a for location of section. **(d)** 3D perspective on the Alps and the Molasse foreland basin illustrating the geodynamic situation between c. 30–20 Ma. Streams with sources in the Central Alps deposited large megafans at the thrust front. These were laterally bordered by bajada fans with sediment sources situated in the frontal Alpine nappes. The discharge within the Molasse foreland basin was oriented towards the NE at that time. Figures a) through c) have been drawn based on Schlunegger and Castelltort²³ using Illustrator 15.1.0 licensed to Uni Bern.

Mesozoic and Neogene times¹⁶. It started with the subduction of the European oceanic lithosphere beneath the Adriatic continental plate and resulted in the closure of the Tethys Ocean sometime during the Late Cretaceous¹⁶. At c. 35 Ma, the collision between both continental plates was completed and followed by the delamination of the European oceanic lithosphere slab beneath the core of the Alps^{16,17}. The result was rapid rock uplift and orogen-parallel extension in the rear of the Alps¹⁶. This was also associated with the build up of topography to the current elevations¹⁸, which in turn caused an increase in the erosion rate and the sediment flux to the adjacent sedimentary basins¹⁹.

The Molasse foreland basin, situated on the northern side of the Alps (Fig. 1a,b), records the erosional evolution of this orogen¹⁶. Surface uplift in the back of the Alps following slab breakoff (Fig. 1c) and the related increase in sediment discharge to the basin¹⁹ was considered to have caused the change from the early underfilled ‘flysch’ to the subsequent overfilled ‘molasse’ type of sedimentation²⁰. This stratigraphic change occurred at c. 30 Ma, as revealed by magneto-polarity stratigraphies²¹. During Molasse times when overfilled conditions prevailed, large sediment fluxes resulted in the construction of alluvial megafans³, which expanded radially into the foreland basin over several tens of kilometers. Close to the apex at the proximal basin border, the megafans are laterally embedded by locally-derived ‘bajada’ fans²¹. While these bajada systems were mainly sourced in the frontal

Alpine nappes, the material of the megafans was derived from both the northern Alpine border and the core of the Alps surrounding the Lepontine dome (Fig. 1a)^{21,22}.

Here, we focus our analyses on the Late Oligocene Rigi megfan conglomerates situated in the north Alpine foreland basin at 47°03'N / 8°29' E (Fig. 1a,b). These deposits chronicle the rise of the Alpine topography and the related changes in erosional mechanisms between 30 and 25 Ma²³. We present data on the structure (e.g., cross-beds, basal contacts, palaeochannel depths) and the grain size of these sediments in order to calculate the fan morphometry including the fan surface slope. We then combine these data with published information about sediment accumulation rates to infer changes in both the rates and the concentrations of the supplied sediment through time. We finally complemented the stratigraphic and sedimentologic dataset with published information about shifts in petrofacies to infer a transient surface response to slab breakoff in the back of the Alps (Fig. 1c,d). We reveal that data about the grain size and the sedimentary structures of conglomerates within a detailed chronological framework²² are essential for linking processes on the Earth's surface with the subduction mechanisms in the mantle.

Results

Among the various sites where alluvial megafan conglomerates have been mapped in the Swiss Molasse, the section at Rigi (Fig. 2a) offers the best exposure where a 30 to 25 Ma-old continuous suite of proximal megafan deposits are encountered. There, the deposits can be grouped into three units, which we refer to as units A to C (Fig. 2b) based on characteristic alternations of lithofacies and the occurrence of key clast types in the conglomerates. Unit A comprises the lowermost 1700 m of the Rigi section and displays an alternation of several m-thick conglomerate beds and mudstone interbeds²⁴. Clast types mainly include carbonate constituents including dolomites, micritic and siliceous limestones, and sandstones that were derived from the frontal Alpine nappes at that time²⁴. Magneto-polarity chronologies reveal that unit A chronicles the evolution of the megafan between 30 and 27 Ma²², and that sediment accumulated at rates between 500 and 600 m/My²². The second unit B, encompassing the thickness interval between 1700 m and 3400 m of the section, comprises an amalgamated stack of dm- to m-thick conglomerate beds. It is characterized by the occurrence of granite clasts that were most likely derived from the crystalline core situated in the rear of the Alps during the Late Oligocene²⁴. Magneto-polarity chronologies reveal that this unit was deposited between 27 and 25–26 Ma²². However, age assignments for the top of unit B strongly depend on how the Rigi magneto-polarity stratigraphy is correlated with the magneto-polarity time scale²². Accordingly, rates of sediment accumulation vary from 800 m/My to >1500 m/My during the time span of unit B deposition²². The deposits of the uppermost c. 200 m of the section, here referred to as unit C, are characterized by alternating mudstones and 3–5 m-thick conglomerate beds with a monomict composition where Penninic flysch clasts are the dominant constituents²⁴. Because Penninic flysch nappes most likely formed the Alpine border during Late Oligocene times, as palinspastic restorations revealed²⁵, unit C had a local provenance^{22,24}. The next paragraphs present the sedimentologic details of each unit.

Base of the section – unit A. Unit A is made up of an alternation of conglomerate beds and mudstone interbeds (Fig. 2b). Individual conglomerates are up to 15 m thick and comprise amalgamated stacks of 2 to 3 m-thick beds that are separated by erosive contacts with m-deep scours. The conglomerates are clast-supported and comprise a massive fabric in most places. Locally, cross-beds with several meters-wide diameters are also visible. Channel depths d scatter around 2–3 m. Individual shallow and deep scours (<1.5 m and >4 m, respectively) also occur. The sizes of the largest clasts D_{max} range between 10–15 cm, while the D_{50} and D_{84} are between 2–6 cm and 3–8 cm large, respectively. The shape of individual clasts range between subrounded and rounded if the classification scheme of Tucker²⁶ (1988) is used for comparison purposes. Mudstone interbeds comprise dm- to m-thick sequences of parallel laminated and cm-thick units. Ripple marks, bioturbation, slickenside fabrics, rootlets and yellow-brown mottling together with caliche nodules also occur. Occasionally, cm-thick mudstones display a dark brown to black colour and contain bone fragments of micro mammals in a few places²².

Petrographic investigations²⁴ revealed that unit A clasts comprise limestone constituents at the base and radiolarite cherts towards the top of the section. Both clast types were most likely derived from the Penninic (limestone clasts) and Austroalpine cover nappes (limestone and radiolarite clasts) that were exposed at the orogenic front prior to 25 Ma according to palinspastic restorations¹⁶. Orientations of gutter casts and axes of cross-beds (Fig. 2b) imply a palaeo-discharge direction that was oriented towards the ENE, i.e., parallel to the basin's axis.

Calculations of fan surface slopes returned values that are generally low. In particular, most of the values range between 0.2° (part α , base of unit A) and 0.4° (part β , top of unit A; Fig. 2b,c). Note, the variations in channel depths d and the spread and uncertainties in the D_{max} values have a minor effect on the results of the fan surface slope calculations. The largest contributions to the scatter in the slope data are due to the two fold differences in assigned values for the Shields²⁷ variable ϕ .

Middle part of the section – unit B. The unit B suite comprises an amalgamated stack of approximately 80 cm- to c. 1.5 m-thick conglomerate beds, forming up to 30 m-thick conglomerate packages (Fig. 2b). Interbedded mudstone beds are rare, and if present they are <1 m thin. The conglomerates reveal a clast-supported and massive fabric with imbrications in places. Where visible, cross-beds with several meters-wide diameters and up to 1.5 m heights also occur. Individual channels were generally 1 m deep. In some places, erosional scours are shallow and only 50 cm deep. At sites where conglomerates are arranged as cross-beds, channel depths exceed 2 m. This has particularly been observed in the lower part of unit B. The sizes of the largest particles D_{max} range between 20–40 cm, while the diameters of the D_{50} and D_{84} measure between 2–6 cm and 3–11 cm, respectively. The clasts are generally subangular if the classification scheme of Tucker²⁶ is used as a basis. Mudstones interbeds comprise cm- to dm-thick sequences of red and yellow mottled units preserving parallel laminations and ripple cross-beds in a few places only. Most of the mudstone interbeds, however, have a massive fabric with slickenside fabrics and caliche nodules.

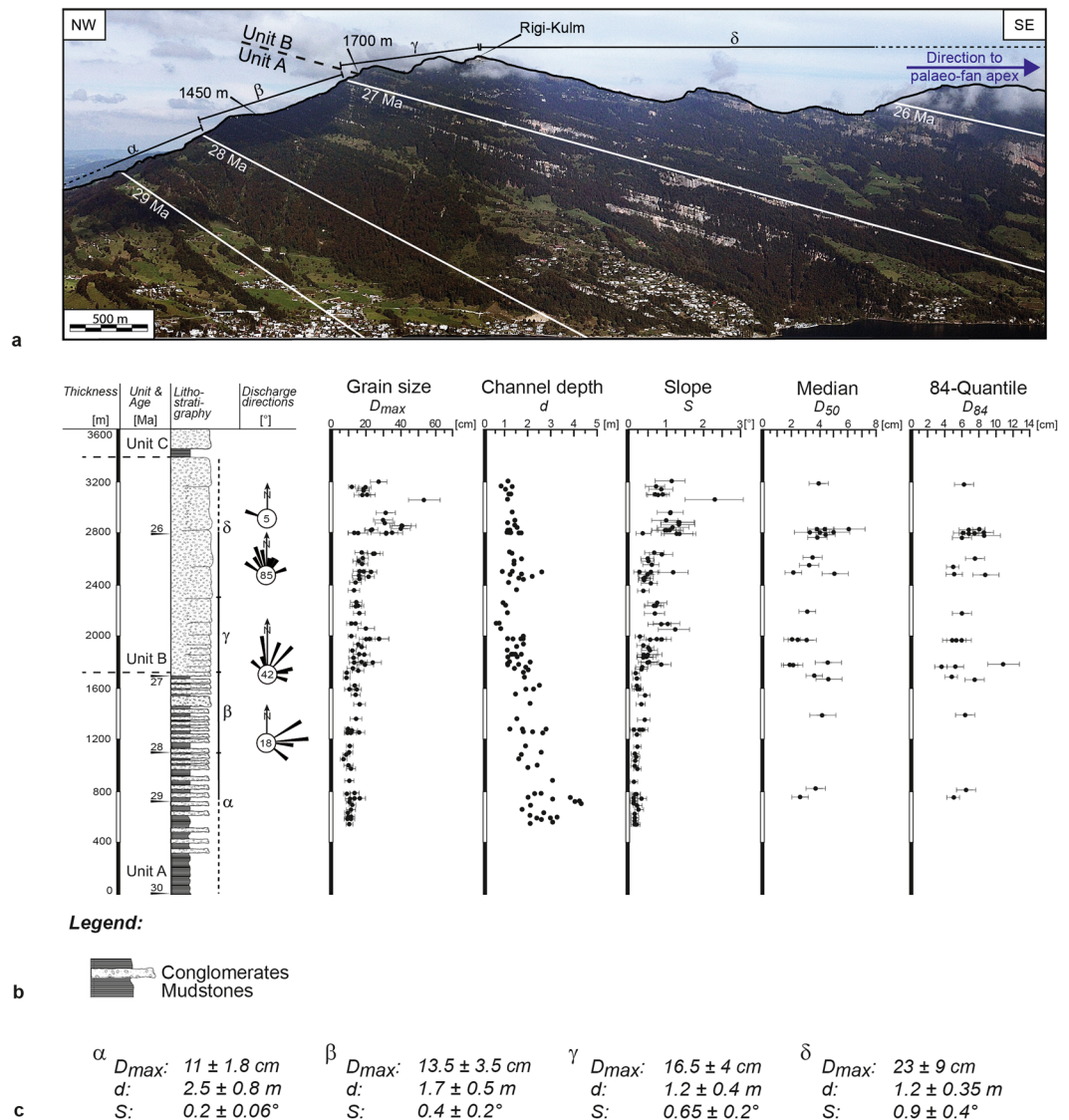


Figure 2. Stratigraphic architecture of the Rigi megafan. **(a)** Photo showing Rigi Mountain. The fan apex deposits crop out on the SE margin of the photo. Accordingly, the deposits at the top of the section (part δ) chronicle a successively more proximal situation. This could potentially blur the interpretation of a progradational trend recorded by the stratigraphic trend of the section. Nevertheless, because shifts towards a more proximal sedimentary environment occurs also on the steep ridge, displayed on the NW margin of the photo (between parts α and γ), the coarsening- and thickening-upward record does include a progradational trend of the Rigi megafan. **(b)** Stratigraphic section²² that is based on a compilation from field-based investigations²⁴. The ages are based on magneto-polarity stratigraphies and have been used to correlate the Rigi conglomerates with other sections in the foreland basin. The figure also shows the results of the sedimentologic investigations, including trends in grain size, channel depths, and palaeo-slopes. Palaeoflow data is based on orientations of gutter casts and cross-beds that we have measured in the field. The number in the circle of the rose diagrams indicates the number of observations. These measures have been combined with literature data^{22,24} into representative rose diagrams. We note that post-depositional compaction could bias the measured channel depths. However, related effects are expected to be larger where the channels are eroded into mudstone (unit A), because mudstones are likely to be compacted to a higher degree than the conglomerates. Therefore, it is likely that underestimates of channel depths in unit A would be larger than in unit B, which contains conglomerates only. The effect is an amplification of the decreasing channel-depth trend illustrated in Fig. 2b. **(c)** Summary of results (largest grain size D_{max} , channel depth d , slope S) for the base (α) and the top (β) of unit A, and also for the base (γ) and the top (δ) of unit B. The subdivisions into α , β , γ and δ of the Rigi section are also displayed on the photo (Fig. 2a) and for the section (Fig. 2b).

Petrographic investigations²⁴ revealed that unit B conglomerates contain red granite clasts that were derived from the basement of the Austroalpine nappes forming the orogenic lid during that time, as revealed from palinspastic restorations of the Central Alps¹⁶. Orientations of imbrications and axes of cross-beds reveal a palaeo-discharge direction that was oriented towards the NNW, i.e., perpendicular to the basin's axis.

During accumulation of unit B, however, fan surface slopes increased from a mean value of c. 0.65° at the base of unit B (part γ of the Rigi section) to >1° towards the top (part δ), albeit with a large scatter (Fig. 2b,c). The steepest slope >2°, calculated for a channel close to the top of unit B, could be related to the foothill of the bordering bajada fans (see below) where distal debris flow processes might have reached the surface of the Rigi megafan.

Top section – unit C. Unit C is characterized by an alternation of mudstones and 3–5 m-thick conglomerate beds with a monomict composition where Penninic flysch clasts are the dominant constituents²⁴. The clasts are generally angular to subrounded. The ensemble of these observations has been used to assign this unit to a bajada-type environment²². Sediment sources were situated at the Alpine front, from where the material was supplied through debris flows processes and high-concentrated floods²¹. Because of the local character of these deposits and since mass wasting processes cannot be described with the Meyer-Peter and Müller²⁸ principles for sediment transport, we will not consider unit C conglomerates in the further analysis.

Summary: evolution from the base to top of the Rigi megafan. In summary, the change from conglomerate-mudstone alternations at the base to the construction of amalgamated conglomerates towards the top of the section at Rigi was associated with a decrease in channel depths from >2 m to <1 m, albeit with a large scatter. These shifts in the stratigraphic architecture were associated with changes in palaeo-flow directions from an axial- to a radial-directed dispersion pattern (Fig. 2). The largest changes in grain size are observed for the D_{max} , which increases from c. 10–15 cm at the base of the sequence, to approximately 20–40 cm towards the top. The mean grain size D_{50} remains stationary between 2–6 cm, while the D_{84} increases slightly from 3–8 cm (with a mean of c. 5.5 cm) at the base to 3–11 cm (with a mean of c. 7 cm) towards the top of the Rigi megafan conglomerates. In addition, the roundness of clasts shifts from between subrounded and rounded at the base of the conglomerate suite to subangular towards the top.

Calculations of fan surface slopes (eq. 6) reveal a large spread, which we partly explain by the scatter in the D_{max} datasets and the measured channel depths d . The largest uncertainties, however, result from assignments of values for the Shields²⁷ variable ϕ . They can vary by up to a factor of 2 depending on reach specific arrangements of clasts (loose and locked boundaries between clasts including hiding and protrusion effects, see methods). While we cannot fully address these complexities with field-based observations, we note that equation 6 returns a trend towards steeper fan surfaces from the base to the top of the section. In particular, the shifts in sedimentation patterns were associated with a >200% steepening of the fan surface from originally <0.3° at the base to >1° towards the top of the conglomerate suite (Fig. 2).

Discussion

The coarsening- and thickening-upward megasequence suggests that the depositional style changed through time from a distal position to a more proximal environment on the megafan^{3,4,21,29}. Supporting evidence is provided by the change in the stratal architecture, the sedimentary fabric and the trend toward less rounded clasts from the base to the top of the Rigi conglomerates. This change in sedimentary fabric and depositional processes was also associated with (i) an upsection trend towards a steeper slope of the fan surface, (ii) an increase of the largest clasts, and (iii) a decrease in channel depths. Such a change in the stratigraphic record could either be explained by the exposure situation where c. 26.5 Ma-old conglomerates (at Rigi-Kulm, Fig. 2a) are farther away from the palaeo-fan apex than the 26 Ma-old deposits²⁴ (on the SE corner of Fig. 2a), or by megafan progradation^{1,5}. However, shifts towards a more proximal environment, where conglomerate beds are more frequent in the stratigraphic suite, are also observed along the steep ridge to the NW of Rigi-Kulm, exposing sediments of parts α through γ in their vertical position (see Fig. 2a). In addition, coarsening- and thickening-upward megasequences are also recorded at contemporaneous sections >15 km farther to the northeast that chronicle the sedimentation pattern of the same dispersal system²², but in a more distal position²². Accordingly, while we cannot fully exclude the possibility that the exposure condition partially explains the aforementioned stratigraphic architecture, the coarsening- and thickening-upward record does include a progradational trend of the Rigi megafan.

Megafan progradation can be explained through: (i) the northward propagation of the Alpine mountain belt and thus of the orogen front^{16,22,25,30}, (ii) a decrease in sediment accumulation rates at constant sediment supply rates⁵, or (iii) an increase in sediment flux at constant or increasing sediment accumulation rates^{1,5,7}. We acknowledge that we cannot fully exclude option one as a driving force for the progradational trend of the megafan, because the Alpine front did shift northward during that time²⁵. However, we do not consider that this mechanism alone explains the inferred shifts towards more proximal sedimentation, because the progradation velocities of the Molasse gravel fronts were faster than the progradation rate of the Alpine thrust front, as palinspastic restorations revealed²⁰. In the same sense, we reject option two as a conceivable mechanism because sediment accumulation rates were increasing and not decreasing up-section, or at least remained constant²². Rather, we consider the change towards more proximal sedimentation paired with the augmentation of the depocenter surface slope, and the increase in maximum grain size as a consequence of a higher sediment supply rate Q ⁴. This interpretation is consistent with the results of numerical models where large-scale coarsening- and thickening-upward megasequences at constant, or increasing sediment accumulation rates point towards a flux- rather than a tectonic-driven change^{1,5}. It appears that such a flux-driven surface response was large enough to result in the burial of the forebulge in the distal foreland, as palaeogeographic reconstructions have shown³¹. This allowed the sediment to disperse over a broader area and to change the sediment dispersion from an axial to a radial pattern³. We thus use the ensemble of these observations to propose that megafan progradation at Rigi was

to a large extent driven by an increase in sediment discharge and not primarily by tectonic processes, as previous authors have claimed^{21,22,24,25}.

Here, we provide evidence for proposing that the temporal increase in sediment flux was also associated with a higher concentration Q_c of the supplied sediment. In this context, we recall that at transport-limited conditions, which is usually the case where megafan progradation is flux driven^{1,3,4}, volumes of supplied sediment per unit time depend on stream power^{5,32}. This variable can be expressed, in the simplest case, as the product between water discharge Q and energy gradient or surface slope S . These relationships, which have been proposed as early as 1955 by Lane³³, have also been derived on theoretical grounds^{5,34}. In addition, they are based on the Bagnold³⁵ bed-load transport formula, and the Darcy-Weisbach equation for computing bedform friction effects on stream flow. Finally, correlations between channel widths and magnitudes of channel forming floods^{36,37}, which commonly correspond to water fluxes during bankfull discharge Q_b events, have also been considered to derive the dependency of sediment flux on stream power^{5,32}. Furthermore, Q_b floods are likely to be strong enough to accomplish equal mobility conditions for all grain sizes, as modern examples of streams in the Swiss Alps have shown³⁸. Accordingly, the relationship between stream power and sediment transport then takes the form:

$$Q_b S = k * Q_s \sum_i p_i D_i \quad (1)$$

where k denotes a proportionality constant, D_i represents the grain size of a particular percentile, and p_i the probability of its occurrence within a grain size population. In addition, it was proposed that at equal mobility conditions, the bed sediment mixture can be reasonably well represented by a single grain size only³⁹. Among the various percentiles representing the grain size D at equal mobility conditions, the D_{50} has been considered to best represent the complete range of grain sizes³⁹. Alternatively, the D_{84} could be of particular interest because this percentile characterizes the bed roughness and the gravel bar structure^{40–42}. Accordingly, eq. (1) simplifies to the following expression:

$$Q_b S = k * Q_s D_{50} \quad (2)$$

Also at transport limited conditions, an increase in stream power results in a larger flux and calibre of the supplied sediment, where:

$$\Delta(Q_b S) = k * \Delta(Q_s D_{50}) \quad (3)$$

Regrouping of eq. (3) and expressing sediment concentration Q_c as the ratio between sediment and water flux $Q_c = Q_s/Q_b$ finally returns an expression that approximates, at first order, the temporal change in Q_c , where:

$$\Delta Q_c = k \Delta \frac{S}{D_{50}}, \quad (4)$$

or alternatively

$$\Delta Q_c = k \Delta \frac{S}{D_{84}} \quad (5)$$

Here, k drops out because it is a constant⁵. Equations (4) and (5) then predict that a change in the concentration of the supplied sediment is proportional to a shift in the ratio between the fan surface slope and the calibre of the supplied sediment. At Rigi, the up-section increase of both grain size percentiles ($\sim 20\%$, from c. 5.5 cm to 7 cm for the D_{84} and zero for the D_{50}) is much less than the change in fan surface slope S , which steepened by $>200\%$ from $<0.3^\circ$ to $>1^\circ$ (Fig. 2). The consequence is a substantial increase in sediment concentration Q_c through time (eqs 4 and 5).

Here, we use the inferred increase in the flux Q_s and the concentration Q_c of the supplied sediment as a basis to propose a change towards faster erosion, and related to this, towards a possible change of the landscape shape in the Alpine hinterland. In this context, we recall that in general, sediment and water flux both increase with the size of the drainage basin A . In addition, both values can be computed, in the simplest case, through the multiplication of A with erosion rate E and precipitation rate P , respectively^{34,43}. Accordingly, an increase in the concentrations of the supplied sediment could then be explained by a decrease in precipitation rates, while erosion rates remained constant. However, such a scenario is very unlikely because neither palaeo-floral⁴⁴ and isotope records from Molasse sediments⁴⁴, nor palaeo-ecological proxy data from deposits in northern continental Europe⁴⁵ do provide evidence for a change in local and regional palaeo-climates, including precipitation^{44,45} during the time when the Rigi conglomerates accumulated²³. Furthermore, shifts towards a warmer palaeoclimate occurred at 25.5 Ma²³, thus 1.5 My later than the change from unit A to B. We rather suggest that the shifts towards larger sediment concentrations, paired with larger sediment fluxes, point towards an increase in erosion rates during the Late Oligocene. We also propose that this inferred increase in erosion rates was associated with a steepening of the Alpine landscape in response to rock uplift driven by lithosphere-scale processes, as outlined in the next paragraph.

The geodynamic evolution of the Alpine orogen can be characterized through the subduction of the European plate beneath the Adiratic continental microplate, which started in Late Cretaceous times¹⁶. Ongoing subduction and closure of the Tethys finally resulted in the collision between both continental plates¹⁶. This was accomplished at c. 35 Ma, when the buoyant European continental plate entered the subduction channel. The differences between the buoyancy forces of the continental part of the European plate and the vertically-directed slab load forces of the subducted oceanic European plate resulted in differential forces, with the result that the subducted

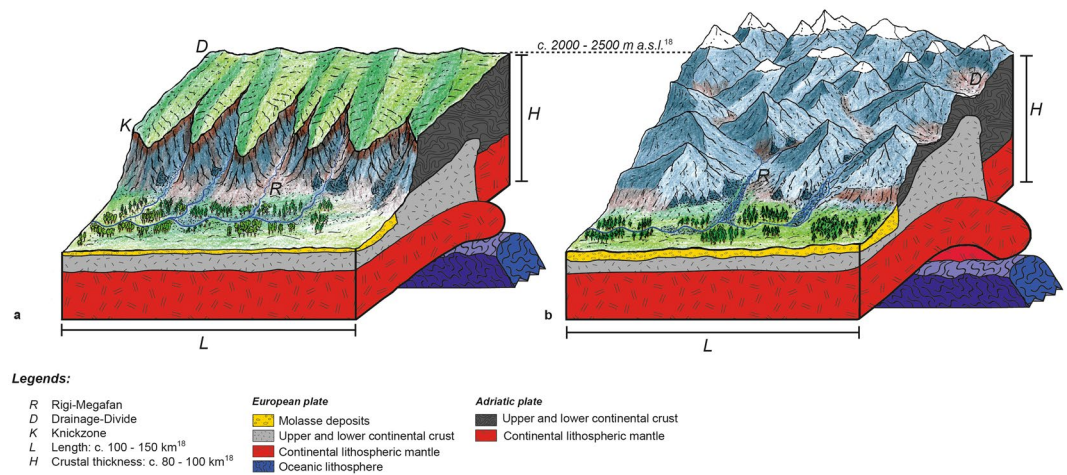


Figure 3. Topographic development of the Alps in response to slab breakoff. **(a)** Situation following slab breakoff. Incipient rise of the Alpine topography caused fluvial incision to initiate at the orogen front as revealed by petrographic investigations and palinspastic reconstructions^{23–25}. This most likely reflects the occurrence of a dissected transient landscape at the orogen front, while the headwaters represented a flat-laying, non- to poorly dissected plateau as clast types from farther south are absent in pre 27 Ma-old deposits²⁴. We suggest that the flat headwater reaches in the south, and the dissected Alpine landscape farther north were separated by a knickzone (K) where most of the erosional work was accomplished. We use this scenario to explain the relatively low fluxes and concentrations of supplied sediment. In the Molasse foreland basin, low sediment fluxes resulted in the establishment of a relatively flat fluvial environment with channels that were confined by a floodplain. See text for further explanations. **(b)** Ongoing uplift promoted headward retreat of knickzones and the shift of the erosional front towards the drainage divide (D) situated in the rear of the Alps, thereby reaching the region where crystalline rocks were exposed. At this stage, the Alpine landscape has reached a steady state situation where ongoing rock uplift is fully compensated by erosion¹⁸, and where the shape of the Alpine landscape has remained stationary. This mechanism explains the delayed arrival of crystalline clasts in the conglomerates and the increase in both the flux and the concentrations of supplied sediment. Sediment concentrations increased until this steady state situation was established. In the Molasse foreland basin, the ensemble of these processes finally caused the Rigi megafan to prograde. See text for further explanations. Please note that both figures have the same scale. Please also note that the topography is exaggerated for illustration purposes. The view on both illustrations is towards the SE.

oceanic slab broke off between 32–30 Ma^{16,17} (Fig. 1c,d). Slab breakoff was followed by rapid rock uplift near the southern limits of the Central Alps and the rise of the Alpine topography to their current elevations between c. 30–25 Ma¹⁸, exactly at the time when the Rigi conglomerates were deposited. Accordingly, we infer that slab breakoff and related surface uplift was the principal driving mechanism for the depocenter progradation at Rigi. We see this mechanism as delayed, and thus transient, surface response where the Alpine streams reacted to the rise of the Alpine topography through headward retreat (Figs 3a,b). The related surface response to slab delamination processes are outlined in the next section.

Channels respond to an increase in rock uplift through steepening their gradients and through an amplification of erosion⁴⁶. If these changes occur in pace with the acceleration in rock uplift rates, i.e., at steady state, then sediment discharge and sediment concentrations will increase at the same pace. Although we cannot discard this possibility with the available grain size dataset, we prefer a transient response to rock uplift. In particular, the predominant occurrence of sedimentary clast types at the bottom of the Rigi section²⁴ suggests that erosion initially started at the orogen front where these lithologies were exposed at that time²⁵. This resulted in the formation of a landscape, where the northern margin of the Alps was characterized by the occurrence of deeply dissected valleys. Farther to the south, the Alpine landscape at that time can be described as a flat-laying, much less dissected plateau¹⁸ (Fig. 3a), similar to the non-dissected, low relief landscape fragments in the modern Central Andes^{47,48}. At 27 Ma, at the base of unit B, the arrival of crystalline clasts in the conglomerates²⁴ suggests that erosion started to affect the Alpine landscape near the drainage divide situated in the rear of the Alps (Fig. 3b), where the corresponding crystalline rocks were exposed at that time¹⁶. Such a southward shift of the sediment sources thus reflects a headward retreat of an erosional front, which was possibly delineated by a knickzone (Fig. 3a). This transient surface response to rock uplift was also associated by an increase in both the flux and the concentration of the supplied sediment (see above), which ultimately reflects a change in the erosional pattern in the Alpine hinterland and a shift towards a steeper landscape (Fig. 3).

If our interpretation is correct, such a proximal record of transient erosional response offers a laboratory for exploring sediment-flux and sediment-concentration dependent surface processes both in the erosional hinterland and in the foreland. Essential in this context are two sets of non-related pieces of information, which includes a temporal calibration of the deposits through detailed chronologies, and a quantification of surface slopes. Indeed, changes in stacking patterns of conglomerates within a detailed chronological framework yields in the identification of shifts in the flux of the supplied sediment only, but this variable alone has no predictive

power on the concentrations of the supplied sediment. Contrariwise, modifications in fan surface slopes provide the basis to estimate shifts in stream power recorded by stratigraphy. The linkage between changes in stream power and sediment supply inferred from the sedimentary record, finally, allowed us to detect possible shifts in concentrations of the supplied sediment during the sedimentation history of the Rigi megafan. It also yields information on the erosional processes and landscape forms in the hinterland where the sediment sources were situated (Fig. 3). Among the various parameters, the rate, the concentration and the granulometric composition of the supplied sediment represent first order independent variables that set the framework for establishing a sedimentary environment in sedimentary basins and that thus control the architecture of stratigraphic records. Our study illustrates that the extraction of the required information from fluvial conglomerates is possible and can be achieved through the quantification of first-order observations in the field, which includes the stacking pattern of conglomerates, channel depths, and data about grain size and clast petrography. As a further implication, our study reveals that causal links between erosional mechanisms operating on the surface, and geodynamic processes occurring at deep crustal levels can be established based on these first-order information preserved in the stratigraphic records.

Methods

Sedimentary environments. We identified the depositional mechanisms from the stacking pattern of conglomerate beds and the sedimentary structures (massive, cross-beds, imbrication, erosional scours) within the lithofacies⁴⁹. Mudstone interbeds were described based on their sedimentary fabric (very fine lamination, ripple crossbeds, mottling, rootlets). In addition, we paid attention on noting the characterization of the surfaces separating conglomerates and mudstone interbeds (vertical scours, lateral fringing and gradual vertical transitions). Palaeo-flow directions were determined from clast imbricates and gutter casts where visible. Finally, the roundness of the clasts was qualitatively estimated using the template by Tucker²⁶ as a basis.

We adapt the results of magneto-polarity²² and micromammal stratigraphies⁵⁰ to constrain the chronological framework of the section. The resulting ages have an uncertainty of less than 0.5 Ma²².

Estimation of palaeo-gradients of channels. Experimental⁵¹, numerical¹⁵ and geomorphic studies⁴ have disclosed positive correlations between energy gradients of streams, or alternatively river slopes S , sediment discharge Q_s , sediment concentration Q_c , and the grain size distribution of gravel bars. Here, we determined these variables and changes thereof using hydrological concepts for bedload entrainment. Related principles predict that a sediment particle with diameter D will be transported if the ratio between the fluid's shear stress τ and the particle's inertia force F ranges between 0.03 and 0.06 (Fig. 4a), which is referred to as the Shields²⁷ variable ϕ . These ϕ values have been applied in numerous studies^{8,52} and consider a broad range of how clasts are arranged in bedload-dominated streams and how this affects the resistance to entrainment (e.g., loose and locked boundaries between clasts including hiding and protrusion effects^{4,53,54}). Because our stream gradient calculations will heavily depend on hydrogeomorphic conditions at bankfull discharge (see below), we employed the range between 0.03 and 0.06 and a mean of 0.046 for the Shields variable ϕ ⁵⁵.

Following Meyer-Peter and Müller²⁸, the fluid's shear stress depends on the hydrological radius, which corresponds to water depths d for wide channels, and the surface slope. As a consequence, the surface slope S can be computed using Shields criteria for the incipient motion of bedload particles paired with data about channel depths and grain size to be collected in the field⁵. Consequently, we used the aforementioned variables to solve eq. 27 by Meyer-Peter and Müller²⁸ for sediment transport:

$$S = \phi \frac{(\rho_s - \rho_w)D}{d\rho_w} \quad (6)$$

Here, the variables ρ_s and ρ_w denote the sediment and water densities, respectively. Slightly modified versions of this equation have been applied in theoretical⁵⁶ and field-based studies⁸. However, a non-unique solution for equation (6) requires that for a given grain size, the corresponding water depth can be independently constrained by observations in the field⁸. Accordingly, we employ the sizes of the maximum clasts D_{max} paired with water depths during bankfull discharge Q_b to calculate the channel gradients S . The next paragraphs justify this approach and present details of how these variables were extracted from conglomerates.

Estimates of water depth d from stratigraphic records. Among the various possibilities of water depth, the situation during bankfull discharge Q_b is considered to offer the most suitable conditions for solving eq. (6) for hydrological and sedimentologic reasons. First, it has been reported that Q_b of streams lays generally, but not always, in the same range as the mean annual floods of these rivers^{39,56}, but we note that return periods of up to 2 years have also been reported⁵⁷. This suggests that Q_b closely approximates the mean annual discharge conditions of a stream. In addition, water shear stresses of Q_b floods are large enough to mobilize nearly all grain size fractions of the bed material, resulting in equal mobility conditions³⁹ including the largest clasts.

From a stratigraphic perspective, sedimentary archives representing Q_b conditions are best recorded and thus visible in the field through distinct arrangements of channels and gravel bars⁵⁸, and have thus been used in comparable studies where the scope was to invert palaeo-slope conditions from stratigraphy⁸. Here, we used two proxies recorded by the Rigi conglomerates to measure water depths during bankfull discharge for the reach scale (Fig. 4b,c). These include the difference between the top of a conglomerate bank and the lowest point of juxtaposed and underlying erosional surfaces, and thicknesses of foresets (α) and longitudinal bars (β). While we cannot address the full range of palaeo-geomorphic complexities upon data collection (under- and overestimates of d related to uncertainties regarding e.g., main vs. tributary channel and post depositional erosion^{56,58}), possible

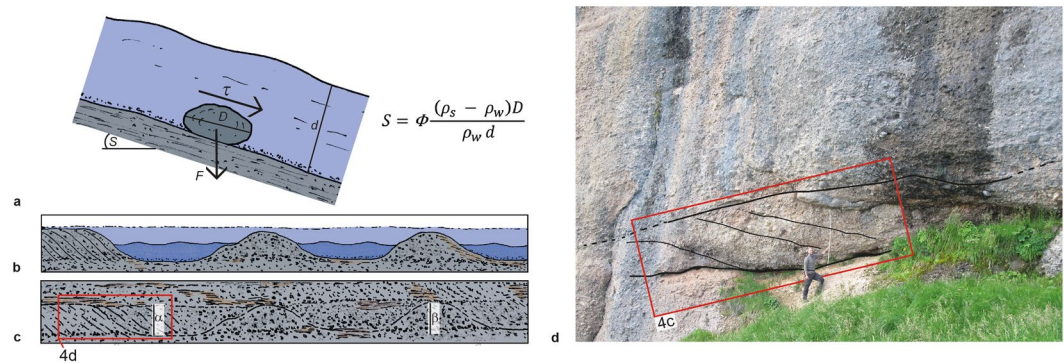


Figure 4. Balances of forces operating on a grain, and channel geometries. **(a)** Force balancing explaining the entrainment of sediment particles. A sediment particle with diameter D will be transported if the ratio between the fluid's shear stress τ and the particle's inertia force F ranges between 0.03 and 0.06, which is the Shields²⁷ variable ϕ . These relationships can then be used to compute slope angles S at equilibrium conditions. The variable d denotes the water depth, g is gravitational acceleration, and ρ_w and ρ_s correspond to water and sediment densities, respectively. **(b)** Section through a braidplain illustrating water depths during low (dark blue) and bankfull discharge (pale blue), when all gravel bars bordering a channel are flooded. In this case, heights of foresets and longitudinal bars define the water depths during bankfull discharge conditions. **(c)** Illustration of how water depths representing bankfull discharge situations are registered in the sedimentologic archive. Accordingly, we measured the difference between the top of a conglomerate bank and the underlying erosional surface (α), and thicknesses of foresets and longitudinal bars (α , β). **(d)** Photo showing sediments of unit B. We used thicknesses of foresets as proxy for channel depth, and we measured the largest clasts (D_{max}) at the base of the foresets. Please see person and meter stick for scale.

uncertainties related to our approach will not alter the general decreasing trend of flow depth from the base to the top of the Rigi section. Furthermore, upon measuring cross bed thicknesses, we paid special attention on selecting those units where topsets are preserved (Fig. 4d), thereby avoiding biases related to post depositional erosion⁵⁹. In the same sense, conglomerate beds with a massive structure, which are indicative for longitudinal bars, are considered as proxy for defining bankfull channel depths only if basal erosional scours at the base and sand lenses on top of these bars are encountered. As sand is frequently deposited on top on longitudinal bars during waning floods, this approach ensures that underestimates related to post-depositional erosion are avoided^{56,58}.

Estimates of grain size D and related distributions from stratigraphic records. While most studies base their analyses on the D_{50} to solve the Meyer-Peter and Müller equation²⁸ for palaeo-slopes^{8,56}, we do not consider this as a valuable approach for the context of this paper, mainly because the Meyer-Peter and Müller equation²⁸ bases on critical conditions for the entrainment of sediment. Indeed, because shear stresses during bankfull discharge floods Q_b are large enough to result in equal mobility conditions of grains across all percentiles including the D_{max} , as field-based data has shown³⁹, the selection of the D_{50} violates the criticality conditions that are included in Shields' criteria. We thus employ the D_{max} to solve equation (6) also because a one-to-one correlation between fan surface slopes and D_{max} have been reported from modern fans at the foothill of the Tucson Mountains and the Aubrey Cliff, AZ⁶⁰. We proceeded by measuring the size of the 4 to 6 largest pebbles and boulders⁵³ at the tip of those bars where we took palaeo-channel depths measurements (Fig. 4d). We then used the mean of these values to infer the size of the D_{max} at these sites.

Ideally, the Meyer-Peter and Müller solution²⁸ for sediment transport applies to grains for which the b - (intermediate) axis has been determined, which decently approximates the nominal diameter of ellipsoidal clasts⁶¹. However, 2D-exposures of conglomerate outcrops preclude a full 3D view on the clasts in the sense that they either expose the a - b or b - c pairs of axes only. Therefore, unambiguous identifications of b -axes are not possible. Among the various possibilities, b/a ratios of c. 0.7 have been measured on >3000 clasts in streams surrounding the Central European Alps³⁸, while no quantitative data is available on neither of the ratios involving the c -axis. Therefore, we avoided data collection in the field that involved measurements of the c -axes because their relationships to the b -axes remain unknown and are thus associated with large and non-quantifiable uncertainties. This leaves us with a strategy, where we measured the longest axis in field. We then accounted for biases related to the exposure conditions through a 15% reduction of the measured lengths, thereby considering the b/a ratios of 0.7³⁸ and the 50% chance of exposure of either axis.

Here, we justify the aforementioned correction through the following thought experiment: Provided that we did indeed measure the b -axis (50% chance), our correction yields in a 15% underestimate of the real length of the b -axis. In case we measured the a -axis (again 50% chance), then our approach overestimates the length of the b -axis by 15%. As the mean of 4 to 6 largest clasts were determined per site, this strategy returns a value that closely corresponds to the b -axis to be considered for the calculation of the slopes (eq. 6). However, since the discussion of this paper mainly focuses on vertical shifts in stratigraphic records and because uncertainties in the D_{max} linearly propagate through our analyses according to eq. (6), we do not consider that a related bias will alter the here presented scenarios and interpretations.

We determined the sediment calibre for c. 50 sites, where we measured a total of approximately 4500 grains using the Wolman⁶² clast counting method. Here, we were faced with the same problem as in the field because digital images do not allow to unequivocally assign a-, b- or c-axes of clasts. However, since we are mainly interested in the vertical grain size trends, we do not consider that this issue will bias related interpretations.

Data Availability. The datasets generated during the current study are available for free from the corresponding author on request.

References

- Armitage, J. J., Duller, R. A., Whittaker, A. C. & Allen, P. A. Transformation of tectonic and climatic signals from source to sedimentary archive. *Nat. Geosci.* **4**, 231–235 (2011).
- Allen, P. A. & Heller, P. L. In *Tectonics of Sedimentary Basins: Recent Advances* (eds Busby, C. & Azor, A.) 111–130 (Wiley-Blackwell, Oxford, 2012).
- Allen, P. A. *et al.* The Qs problem: Sediment volumetric balance of proximal foreland basin systems. *Sedimentology* **60**, 102–130 (2013).
- Church, M. Bed material transport and the morphology of alluvial river channels. *Ann. Rev. Earth Planet. Sci.* **34**, 325–354 (2006).
- Paola, C., Heller, P. L. & Angevine, C. The large-scale dynamics of grain-size variation in alluvial basins, 1: Theory. *Basin Res.* **4**, 73–90 (1992).
- Leeder, M. K., Harris, T. & Krikby, M. J. Sediment supply and climate change: implications for basin stratigraphy. *Basin Res.* **10**, 7–18 (1998).
- Whittaker, A. C. *et al.* Decoding down- stream trends in stratigraphic grain size as a function of tectonic subsidence and sediment supply. *GSA Bull.* **123**, 1363–1382 (2011).
- Duller, R. A. *et al.* From grain size to tectonics. *J. Geophys. Res. - Earth Surf.* **115**, F03022 (2012).
- Parsons, A., Michael, N. A., Whittaker, A., Duller, R. & Allen, P. A. Grain size trends reveal the late orogenic tectonic and erosional history of the south-central Pyrenees, Spain. *J. Geol. Soc. London* **169**, 111–114 (2012).
- Michael, N. M., Whittaker, A. C. & Allen, P. A. The functioning of sediment routing systems using a mass balance approach: Example from the Eocene of the southern Pyrenees. *J. Geol.* **121**, 581–606 (2013).
- Michael, N. A., Whittaker, A. C., Carter, A. & Allen, P. A. Volumetric budget and grain-size fractionation of a geological sediment routing system: Eocene Escanilla Formation, south-central Pyrenees. *GSA Bull.* **126**, 585–599 (2014).
- Romans, B. W., Castelltort, S., Covault, J. A., Fildani, A. & Walsh, J. P. Environmental signal propagation in sedimentary systems across timescales. *Earth Sci. Rev.* **153**, 7–29 (2016).
- Allen, P. A. *et al.* Fractionation of grain size in terrestrial sediment routing systems. *Basin Res.* **29**, 180–202 (2017).
- D'Arcy, M., Whittaker, A. C. & Roda-Boluda, D. C. Measuring alluvial fan sensitivity to past climate changes using a self-similarity approach to grain-size fining, Death Valley, California. *Sedimentology* **64**, 388–424 (2016).
- Hinderer, M. *et al.* River loads and modern denudation of the Alps – A review. *Earth Sci. Rev.* **118**, 11–44 (2013).
- Schmid, S. M., Pfiffner, O. A., Froitzheim, N., Schönborn, G. & Kissling, E. Geophysical-geological transect and tectonic evolution of the Swiss-Italian Alps. *Tectonics* **15**, 1036–1064 (1996).
- Davis, J. H. & von Blanckenburg, F. Slab breakoff: a model of lithospheric detachment and its test in the magmatism and deformation of collisional orogens. *Earth Planet. Sci. Lett.* **129**, 85–102 (1994).
- Schlunegger, R. & Kissling, E. Slab rollback orogeny in the Alps and evolution of the Swiss Molasse Basin. *Nat. Comm.* **6**, 8605 (2015).
- Sinclair, H. D. Flysch to Molasse transition in peripheral foreland basins: the role of the passive margin versus slab breakoff. *Geology* **25**, 1123–1126 (1997).
- Sinclair, H. D. & Allen, P. A. Vertical versus horizontal motions in the Alpine orogenic wedge: stratigraphic response in the foreland basin. *Basin Res.* **4**, 215–232 (1992).
- Kempf, O., Matter, A., Burbank, D. W. & Mange, M. Depositional and structural evolution of a foreland basin margin in a magnetostratigraphic framework; the eastern Swiss Molasse Basin. *Int. J. Earth Sci.* **88**, 253–275 (1999).
- Schlunegger, F., Matter, A., Burbank, D. W. & Klaper, E. M. Magnetostratigraphic constraints on relationships between evolution of the central Swiss Molasse Basin and Alpine orogenic events. *Geol. Soc. Am. Bull.* **109**, 225–241 (1997).
- Schlunegger, F. & Castelltort, S. Immediate and delayed signal of slab breakoff in Oligo/Miocene Molasse deposits from the European Alps. *Sci. Rep.* **6**, 31010 (2016).
- Stürm, B. Die Rigischüttung. Sedimentpetrographie, Sedimentologie, Paläogeographie, Tektonik. PhD thesis, Univ. Zürich. Switzerland, 98 p (1973).
- Pfiffner, O. A. In *Foreland Basins* Vol. 8 (eds Allen, P. A. & Homewood, P.) 219–228 (Int. As. Sed. Spec. Publ., 1986).
- Tucker, M. E. *Techniques in Sedimentology*. Blackwell Sci. Publ., 394 pp (1988).
- Shields, A. Anwendung der Ähnlichkeitsmechanik und der Turbulenzforschung auf die Geschiebebewegung. Mitt. Preuss. Versuch. Wasserbau Schiffbau, 26, (Berlin) (1936).
- Meyer-Peter, E. & Müller, R. Formulas for bedload transport. Proceedings of the 2nd meeting of the Int. Assoc. Hydraul. Struct. Res., Stockholm, Sweden. Appendix 2, 39–64 (1948).
- Miall, A. D. Architectural element analysis: a new method of facies analysis applied to fluvial deposits. *Earth Sci. Rev.* **22**, 261–308 (1985).
- Horton, B. K. & DeCelles, P. G. Modern and ancient fluvial megafans in the foreland basin system of the central Andes, southern Bolivia: implications for drainage network evolution in fold-thrust belts. *Basin Res.* **13**, 43–63 (2001).
- Schlunegger, F., Jordan, T. E. & Klaper, E. M. Controls of erosional denudation in the orogen on foreland basin evolution: The Oligocene central Swiss Molasse Basin as an example. *Tectonics* **16**, 823–840 (1997).
- Allen, P. A. & Densmore, A. L. Sediment flux from an uplifting block. *Basin Res.* **12**, 367–380 (2000).
- Lane, E. W. The importance of fluvial morphology in river hydraulic engineering. *Proc. Amer. Soc. Civil. Eng.* **81**, 1–17 (1955).
- Tucker, G. E. & Slingerland, R. Predicting sediment flux from fold and thrust belts. *Basin Res.* **8**, 329–349 (1996).
- Bagnold, R. A. An approach to the sediment transport problem from general physics. *Prof. Pap. U.S. Geol. Surv.* **422-I** (1966).
- Yalin, M. S. *Mechanics of Sediment Transport*. 2nd edn. Pergamon Press, New York (1977).
- Chaudhry, M. H. *Applied Hydraulic Transients* (3rd ed.), Springer. p. 45 (2013).
- Litty, C. & Schlunegger, F. Controls on Pebbles' size and shape in streams of the Swiss Alps. *J. Geol.* **125**, 101–112 (2017).
- Van den Berg, J. H. Prediction of alluvial channel pattern of perennial rivers. *Geomorphology* **12**, 259–279 (1995).
- Howard, A. D. In *Thresholds in Geomorphology* (eds Coates, D. R. & Vitek, J. D.) 227–258 (Allen and Unwin, Boston, M. A., 1980).
- Hey, R. D. & Thorne, C. R. Stable channels with mobile gravel beds. *J. Hydr. Eng.* **112**, 671–689 (1986).
- Grant, G. E., Swanson, F. J. & Wolman, M. G. Pattern and origin of stepped-bed morphology in high gradient streams, western Cascades, Oregon. *GSA Bull.* **102**, 340–352 (1990).
- Tucker, G. E. & Slingerland, R. Drainage basin responses to climate change. *Wat. Res. Res.* **88**, 2031–2047 (1997).
- Berger, J. P. Paléontologie de la Molasse de Suisse Occidentale, Taxonomie, Biostratigraphie, Paléoécologie, Paléogéographie et Paléoclimatologie. Habilitation thesis, 405 p. (Univ. Fribourg, 1992).

45. Mosbrugger, V., Utescher, T. & Dilcher, D. L. Cenozoic continental climatic evolution of Central Europe. *PNAS* **102**, 14964–14969 (2005).
46. Whipple, K. X. & Tucker, G. E. Dynamics of the stream-power river incision model: Implications for height limits of mountain ranges, landscape response timescales, and research needs. *J. Geophys. Res.* **104**, 17661–17647 (1999).
47. Whipple, K. X. & Gasparini, N. M. Tectonic control of topography, rainfall patterns, and erosion during rapid post-12 Ma uplift of the Bolivian Andes. *Lithosphere* **6**, 251–268 (2014).
48. Whipple, K. X. Bedrock rivers and the geomorphology of active orogens. *Ann. Rev. Earth Planet. Sci.* **32**, 151–185 (2004).
49. Miall, A. D. Lithofacies types and vertical profile models in braided river deposits: a summary. *Fluvial Sedimentology. Can. Soc. Petrol. Geol. Mem.* **5**, 597–604 (1978).
50. Engesser, B. & Kälin, D. *Eomys helveticus* n. sp. and *Eomys schluneggeri* n. sp., two new small eomyids of the Chattian (MP 25/MP 26) subalpine Lower Freshwater Molasse of Switzerland. *Fossil Imprint* **73**, 213–224 (2017).
51. Whipple, K. W., Parker, G., Paola, C. & Mohrig, D. Channel dynamics, sediment transport, and the slope of alluvial fans: experimental study. *J. Geology* **106**, 677–694 (1998).
52. Attal, M., Tucker, G. E., Whittaker, A. C., Cowie, P. A. & Roberts, G. P. Modeling fluvial incision and transient landscape evolution: influence of dynamic channel adjustment. *J. Geophys. Res.* **113**, F03013 (2008).
53. Church, M. Palaeohydrological Reconstructions from a Holocene Valley Fill. *Fluvial Sedimentology* **5**, 743–772 (1997).
54. Buffington, J. M. & Montgomery, D. R. A systematic analysis of eight decades of incipient motion studies, with special reference to gravel-bedded rivers. *Water Res. Res.* **33**, 1993–2029 (1997).
55. Andrews, E. D. Bed-material entrainment and hydraulic geometry of gravel-bed rivers in Colorado. *GSA Bull.* **95**, 371–378 (1984).
56. Paola, C. & Mohring, D. Palaeohydraulics revisited: palaeoslope estimation in coarse-grained braided rivers. *Basin Res.* **8**, 243–254 (1996).
57. Williams, G. P. Bank-full discharge of rivers. *Water Res. Res.* **14**, 1141–1154 (1978).
58. Stock, J. D., Schmidt, K. M. & Miller, D. M. Controls on alluvial fan long-profiles. *U.S. Geol. Surv.* **12**, 619–640 (2008).
59. Paola, C. & Borgman, L. Reconstructing random topography from preserved stratification. *Sedimentology* **38**, 553–565 (1991).
60. Blissenbach, L. Relation of Surface Angle Distribution on to Particle. *J. Sediment. Petrol.* **22**, 25–28 (1952).
61. Koster, E. H. The Ellipsoidal Form of Clasts with Practical Applications to Fabric and Size Analyses of Fluvial Gravels. *Can. J. Earth Sci.* **17**, 1725–1739 (1980).
62. Wolman, M. A method of sampling coarse river-bed material. *Trans. Am. Geophys. Union* **35**, 951–956 (1954).

Acknowledgements

This research was funded through the Swiss National Science Foundation.

Author Contributions

F.S. designed the study. P.G. carried out the experiments, collected and interpreted the data with support by F.S., and draw the figures. The handcrafted Figures 1c, 3a–b, 4a–c were done by P.G. The photos of Figures 2a and 4d were taken by P.G. and F.S., respectively. F.S. and P.G. wrote the text.

Additional Information

Competing Interests: The authors declare that they have no competing interests.

Publisher's note: Springer Nature remains neutral with regard to jurisdictional claims in published maps and institutional affiliations.



Open Access This article is licensed under a Creative Commons Attribution 4.0 International License, which permits use, sharing, adaptation, distribution and reproduction in any medium or format, as long as you give appropriate credit to the original author(s) and the source, provide a link to the Creative Commons license, and indicate if changes were made. The images or other third party material in this article are included in the article's Creative Commons license, unless indicated otherwise in a credit line to the material. If material is not included in the article's Creative Commons license and your intended use is not permitted by statutory regulation or exceeds the permitted use, you will need to obtain permission directly from the copyright holder. To view a copy of this license, visit <http://creativecommons.org/licenses/by/4.0/>.

© The Author(s) 2017